LAWRENCE
LIVERMORE
NATIONAL
LABORATORY

LLNL-TR-443691

Reflux physics and an operational scenario for the spheromak

E. B. Hooper

July 20, 2010

Disclaimer

This work performed under the auspices of the U.S. Department of Energy by Lawrence Livermore National Laboratory under Contract DE-AC52-07NA27344.

Technical Note

DATE: July 19, 2010

TO: General

FROM: E. B. Hooper

SUBJECT: Reflux physics and an operational scenario for the spheromak

I. INTRODUCTION

The spheromak [1] is a toroidal magnetic confinement geometry for plasma with most of the magnetic field generated by internal currents. It has been demonstrated to have excellent energy confinement properties: A peak electron temperature of 0.4 keV was achieved in the Compact Torus Experiment (CTX) experiment [2] and of 0.5 keV in the Sustained Spheromak Physics Experiment (SSPX) [3]. In both cases the plasmas were decaying slowly following formation and (in SSPX) sustainment by coaxial helicity injection (CHI) [4]. In SSPX, power balance analysis during this operational phase yielded electron thermal conductivities in the core plasma in the range of 1-10 m^2/s [5, 6], comparable to the tokamak L-mode. These results motivate the consideration of possible operating scenarios for future fusion experiments or even reactors.

Formation and sustainment of the spheromak configuration by CHI is due to a n=1 magnetohydrodynamic (MHD) mode driven by the current column along the geometric axis, as has been demonstrated in numerous experiments [CTX, FACT, SPHEX, SSPX]. Energy confinement during formation and sustainment has been found to be poor. Resistive MHD simulations [7, 8] show that the MHD mode generates reconnection events which convert injected toroidal magnetic flux into poloidal magnetic flux resulting in an amplification of the bias poloidal magnetic flux in the "gun." These relaxation events result in the magnetic configuration relaxing into the spheromak geometry. The relaxation and reconnection events open magnetic surfaces, however, allowing the field lines to reach the walls of the confining flux conserver. The non-axisymmetric magnetic field perturbations are < 10% and the perturbation of the axisymmetric field is even smaller; consequently the geometry is properly described as a mean-field spheromak. The electron temperature is determined by transport along the field lines, however, and is typically < 40 eV. The field becomes highly symmetric in the slowly-decaying phase, allowing closed flux surfaces to form resulting in good confinement and high electron temperatures.

The spheromak could be sustained by carefully tailored axisymmetric processes, e.g. using neutral beam injection [9, 10], but this has been not been addressed experimentally. As a result, there is no presently demonstrated means of sustaining a high-temperature spheromak at high temperature. An alternative approach is to operate in a quasi-steady state mode termed "refluxing," in which

the spheromak is formed by CHI followed by a high-confinement phase. When the field has partially decayed, the plasma would be rebuilt by another CHI pulse. In principal, this mode of operation could be extended indefinitely. This paper considers the physics of this operation with the goal of evaluating how an experiment might be successfully operated.

II. REFLUXING OVERVIEW

A schematic time history of the refluxing scenario is shown in Fig. 1. In the example shown, the toroidal current is allowed to decay by a relatively small amount; the optimal level will depend on confinement scaling with magnetic

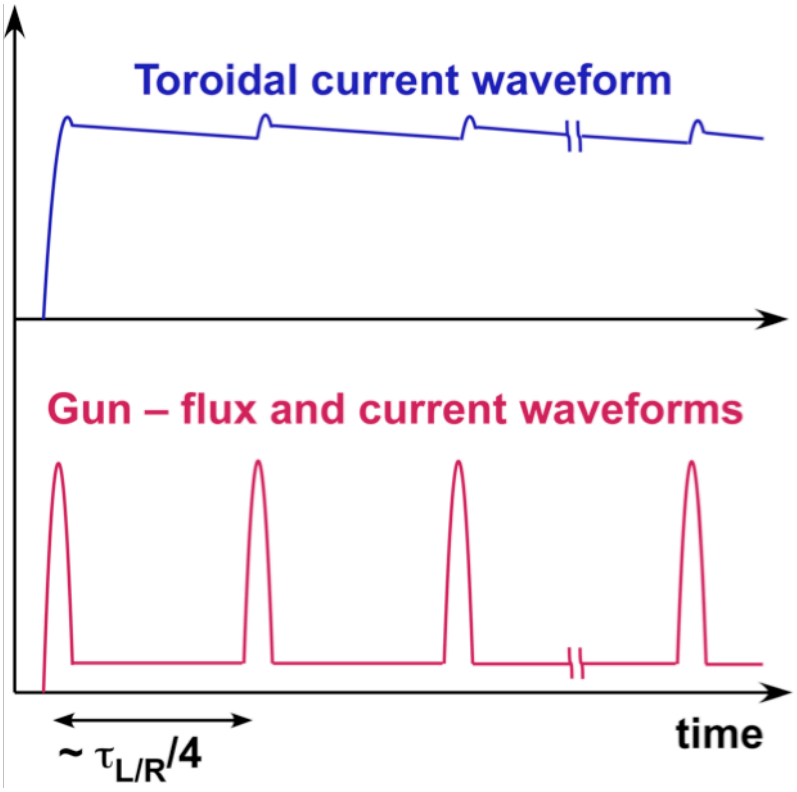

Fig. 1. Refluxing schematic {APS-DPP2009/APS-DPP2009.ppt}*.

field and power balance considerations, which are presently poorly understood. Reactor feasibility will also depend on the effects of the time-varying forces and heat flow on material used in the device [reference?]. We leave these issues to future studies.

The poloidal flux in the spheromak arises from an effective amplification of an applied bias flux by CHI and is an important parameter [11] for both physics and reactor considerations. In SSPX this amplification was limited to less than ~ 5; at stronger drives the amplification was found to saturate [12] for reasons which are not well understood but may include intense wall interactions. Although it may be possible to increase this limit, e.g. by gun geometry

*The curly brackets are used to identify the figure for future use

optimization, it seems unlikely that it will reach the factor of ~50 required to limit power losses in the edge plasma in a reactor [13]. Modeling and simulations [11] point to an alternate means to satisfy this condition on the volume of plasma in the edge plasma: reducing the bias flux and gun current together once the spheromak equilibrium is formed. This reduces the edge plasma volume proportionally, dropping the input power losses while maintaining the value of $\lambda = \mu_0 j/B$ on the open field lines at the value needed to maintain MHD stability [5]. The gun flux and current waveforms shown schematically in Fig. 1 illustrates this scenario.

In the following sections resistive MHD simulations are carried out for this scenario. However, 3D, full-device simulations for a strongly driven spheromak take extensive computer time. Thus, to more fully examine the physics, an integrated physics model (IPM) is developed and benchmarked against the simulations. It aids further development of the underlying physics and allows exploration of the behavior of the refluxing scenario. Results from the IPM are then used to modify the time history and operating scenarios for a second simulation.

III. SPHEROMAK FORMATION

The NIMROD MHD code has been used extensively spheromak simulations, especially of SSPX. (See [14, 7, 8] and references therein.) In this section we consider the formation and buildup of the spheromak. The resulting plasma is used to begin both of the refluxing scenarios. The modeling is done in the SSPX geometry as extensive simulations have been compared with experimental data, finding good semi-quantitative agreement on most parameters and good quantitative agreement on many. Optimization of the gun and flux conserver geometry will be left to a future exercise.

A. Resistive MHD simulations

For the scenario chosen here, we choose an operating point at $\lambda_{gun} = \mu_0 I_{gun}/\psi_{gun} = 25\ m^{-1}$. This is above the value at which the SSPX experiment observed saturation in the buildup [12]. This saturation issue is assumed to be resolved sufficiently to allow extending the buildup to the poloidal flux amplification studied here, reaching a flux amplification > 7 using CHI. The simulation starts with a bias flux of 50 mWb, approximately the maximum used in SSPX. The cross-field thermal conductivity is set to 20 m^2/s, although with the flux surfaces open much of the time, this value has little impact. The gun current and voltage during this buildup phase are shown in Fig. 2. Figure 3 shows the evolution of poloidal flux and temperature during this phase.

Several comments are in order:

- The buildup is due to reconnection events which convert the injected toroidal flux into poloidal flux [7, 8]. These events, which occur when the

symmetry-breaking n=1 mode amplitude becomes large, destroy magnetic surfaces causing a rapid loss of thermal energy to the walls surrounding the spheromak. The voltage spikes arise from the large inductive "kick" when the current rearranges during the event [7]. The mode amplitude also drops rapidly during the event, allowing the surfaces to begin healing until the next event. The "sawtooth-like" behavior of the temperature in Fig. 3 reflects this process.

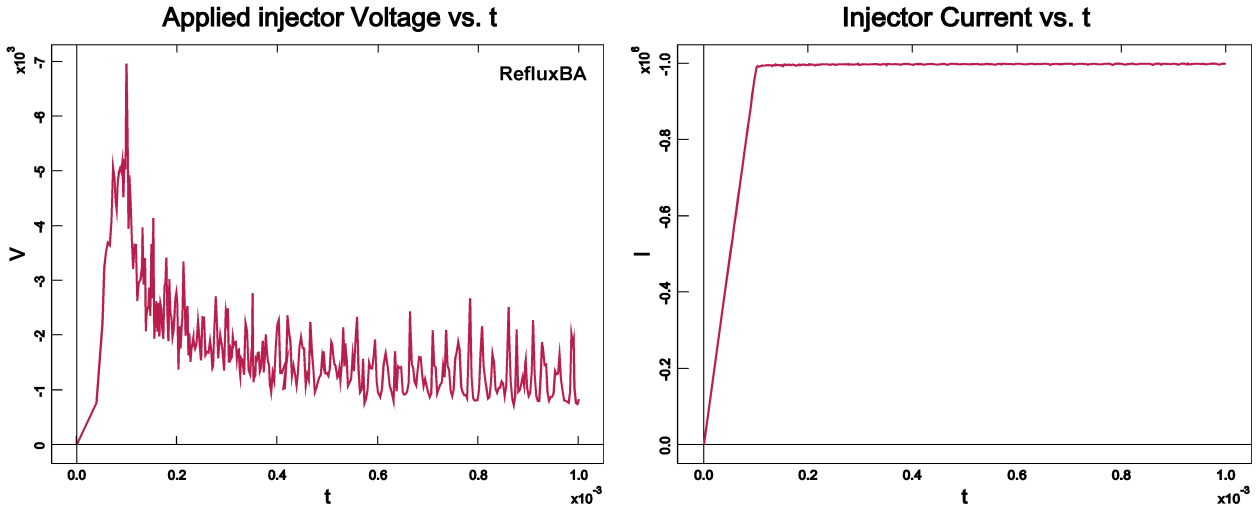

Fig. 2. Gun voltage and current during the formation phase {reflux-buildup/refluxBA_volt.tif, refluxBA_current.tif}.

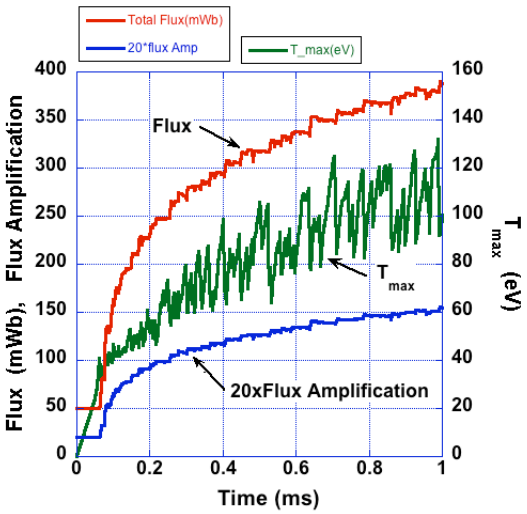

Fig. 3. Buildup phase of the spheromak, showing flux, poloidal flux amplification, and temperature on the magnetic axis. Flux amplification is defined as [flux(mag. axis) + bias flux]/bias flux [11]. The maximum flux amplification achieved during the buildup phase is 7.7. {Reflux1/RefluxBA/RefluxBA-buildup.tif}

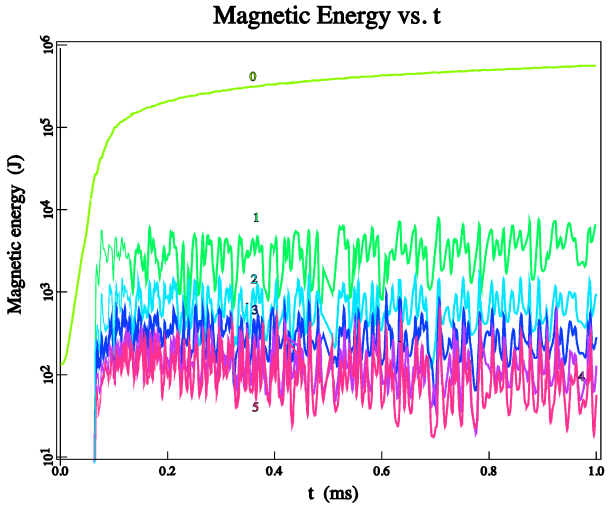

Fig. 4. Magnetic energy in modes n= 0 (axisymmetric) to 5. These are the modes included in the simulation. {reflux-buildup/refluxBA_en_log-t.tif}

- The flux build-up has clearly not saturated at 1 ms. However the power input to form the spheromak (including most of the associated magnetic field) is substantial. The total power input, discussed below, can be seen from Fig. 2 to be > 1GW (1 MJ/ms). The total magnetic field energy, Fig. 4, is 0.52 MJ. The actual rate of increase of the axisymmetric magnetic energy at 1 ms, however, is about 0.035 MJ/ms, an efficiency of only 6.7% consistent with experiment. Because the simulations take extensive computational time, no attempt has been made to optimize the efficiency, e.g. by varying the buildup rate or varying the gun and flux-conserver geometry. Never-the-less, it is clear that there is an increasing cost as the buildup approaches saturation and the rate of flux amplification decreases. For present purposes the buildup calculation is ended at 1 ms.

- Power and helicity injection are associated with several loss channels in the plasma [15]. From the prospect of a mean-field, axisymmetric approximation, these are (1) buildup of the magnetic field and plasma heat with subsequent resistive decay, (2) reconnection events, and (3) ohmic losses in the edge plasma. These edge losses are estimated below.

Figure 5 shows an example of the flux surfaces calculated from the n=0 component of the magnetic field. The ohmic heating of the edge plasma is dominated by the smallest area of the current path in the edge, which occurs at the midplane where the radius is R_{col} =0.0545 m. We can thus estimate the resistivity as $\eta L_{col}/\pi R_{col}^2$, with the column length L_{col}≈0.5 m. The resistivity is $7.5\times10^{-4}T^{-3/2}$ Ω-m ≈ 4.6x10^{-6} Ω-m, and the resistance about 2.5x10^{-4} Ω, consistent with although somewhat less than the SSPX experiment. At a gun current of 1 MA, the gun voltage due to edge losses is 240 V resulting in about 0.24 GW of heating, roughly 1/4 of the total input. As we will see, this is much larger than the heating due to ohmic losses in the final, slowly decaying spheromak.

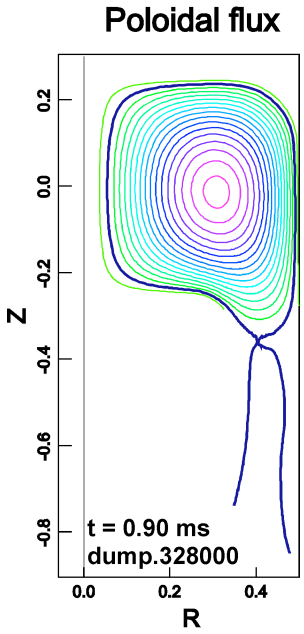

Fig. 5. Axisymmetric, poloidal magnetic flux surfaces at t = 0.90 ms. {refluxBA_polfl.tif}

B. Integrated physics model

The IPM is based on the Corsica/Caltrans code [16, 17] which uses an axisymmetric (mean-field) approximation including models for current-drive, transport, heating, and other effects which may result from non- axisymmetric physics. Current is driven by a loop voltage (axisymmetric electric field) and hyper-resistivity [18] due to from the non-axisymmetric turbulence. Heating results both from the current driven by the loop voltage and from the turbulence that drives the hyper-resistivity. Cross field energy transport is modeled by a thermal conductivity which is taken to be a constant in the absence of experimental understanding of the mechanisms involved. In regions where the magnetic fluctuations are strong enough to generate a hyper-resistive current drive, field lines are assumed open so the energy transport across the mean-field surfaces also includes a Rechester-Rosenbluth approximation [19]. The results provide further insight into the results seen in the simulations and can be used to extend those results to other plasma parameters. The model is described in more detail in the Appendix.

As Corsica assumes closed flux surfaces in the mean-field approximation it is unable to model the plasma initiation in the gun and its subsequent "bubble-burst" into the flux-conserver volume [20]. Instead, the integrated modeling is initiated by a fit to the simulation flux and temperature, Fig. 3, at 0.1 ms. The evolution of the flux and temperature during the buildup to 1 ms are fitted to yield the "best" values of the parameters Λ and $|\delta B/B|^2$. (These values are kept constant for helicity injection into the fraction of stochastic volume on the plasma edge which is stochastic at later times.) As in the MHD simulation, the cross-field thermal conductivity = 20 m^2/s. The best fits during the buildup are found to be $\Lambda = 0.273$ V-Wb and $|\delta B/B|^2 = 1.5\text{x}10^{-3}$. The latter corresponds to a time-

averaged fluctuation level of 3.9×10^{-2}, quite similar to experimental observations. The fits to the buildup evolution are shown in Fig. 6.

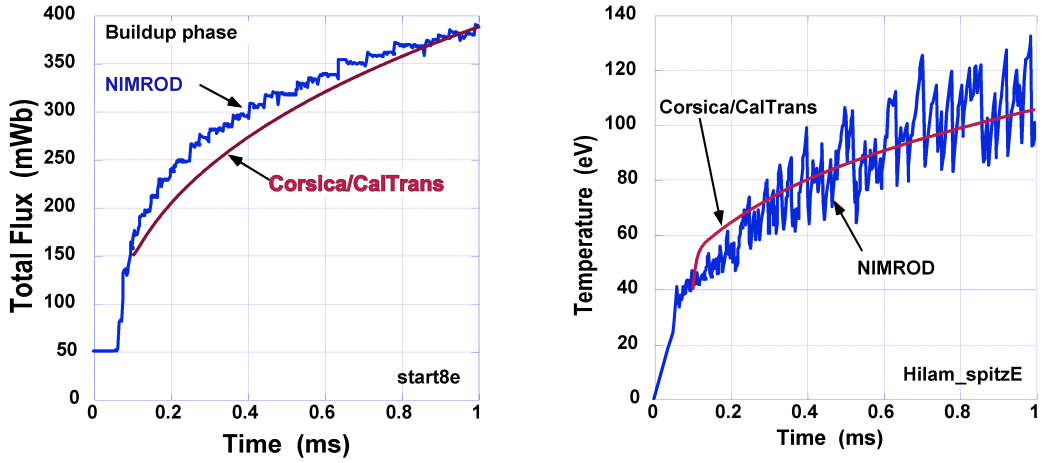

(a) (b)

Fig. 6. Comparison between the integrated modeling result and NIMROD simulation. (a) Poloidal flux. (b) Temperature. {reflux-buildup/Reflux_BA-buildup, Corsica-spitz/RefluxBA_T-buildup spitz.tif}

IV. GUN FLUX AND CURRENT REDUCTION

As seen in Fig. 1, the next phase of the pulse involves reducing the gun flux and current to values that optimize the controlled decay. Two "transitions" are done to satisfy two different physics goals: (1) lowering the gun (bias) flux and current minimizes the volume of the edge plasma and (2) lowering the value of λ_g reduces the instability drive from the central column current. These could be done simultaneously, but in order to understand the physics consequences, we do them in sequence. The order of the two transitions affects the plasma behavior in large measure because they are occur more rapidly than the current diffusion time in the core plasma when "good" flux surfaces are present. If the surfaces are open, the effective current diffusion time is considerably reduced.

In order to distinguish the two options in the following, they will be termed REDUC-12 when (1) is done before (2) and REDUC-21 when (2) precedes (1).

A. REDUC-12 (MHD simulation)

In REDUCT-12, transition (1) is done in the 1 ms following the plasma formation, followed by transition (2) in the following 0.1 ms. The reduction of gun flux and current is done over 1 ms using the same evolution in time as assumed in Ref. 11:

$$\psi_{gun}, I_{gun} \sim 1 + (f_0 - 1)(t - t_1)^2 (3t_2 - t_1 - 2t) / (t_2 - t_1)^3$$

This function on the rhs decreases from 1 at $t = t_1$ to f_0 at $t = t_2$, with zero derivatives at t_1 and t_2. We set t_1=1 ms. t_2=2 ms, and f_0=0.155 to bring the final flux amplification to ≈ 50. The resulting flux and temperature is shown in Fig. 7; the flux amplification reaches 46, slightly short of the goal. Note that the flux amplification and reconnection events continue until the flux amplification has increased by about 20%, after which flux surfaces begin to close and the maximum temperature (on the magnetic axis) begins to increase smoothly.

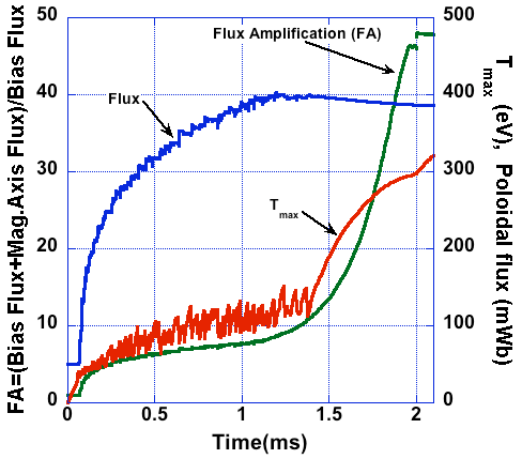

Fig. 7. Time history of buildup (0-1 ms), flux-amplification increase (1-2 ms), and reduction of λ_g from 25 m^{-1} to 10 m^{-1} (2.0-2.1 ms) in the Nimrod simulation REDUCT-12, showing the peak temperature, poloidal flux, and flux amplification. {Reflux-decay/RefluxBA2 copy.tif}

At 2.0 ms the bias flux is fixed and λ_g reduced from 25 m^{-1} to 10 m^{-1} over 0.1 ms. (The thermal conductivity is decreased to 5 m^2/s.) The resulting evolution is included in the figure.

The poloidal-flux surfaces for the mean-field spheromak at 2 ms are shown in Fig. 8a. However, the actual surfaces are not closed all the way to the separatrix. A Poincaré (puncture) plot for the field at 2 ms is shown in Fig. 8b. The amplitude of magnetic modes excited near the separatrix is large enough to destroy the surfaces near the separatrix. This, in turn, affects the thermal confinement. In the calculation up to 2.0 ms, the thermal conductivity is assumed to be $\chi_\perp = 20\ m^2/s$, but the reduced minor radius of "good" surfaces allows more losses than anticipated The quantitative consequences will be discussed in the section on controlled decay.

Figure 9 shows the mean-field q and λ_g profiles from 1.0 - 2.1 ms. Note that the safety factor reaches unity after about 1.5 ms. One might expect that an internal m=1, n=1 mode might be generated, but the mode plots (Fig. 10) indicate the strongest activity for the n=1 mode is near the separatrix.

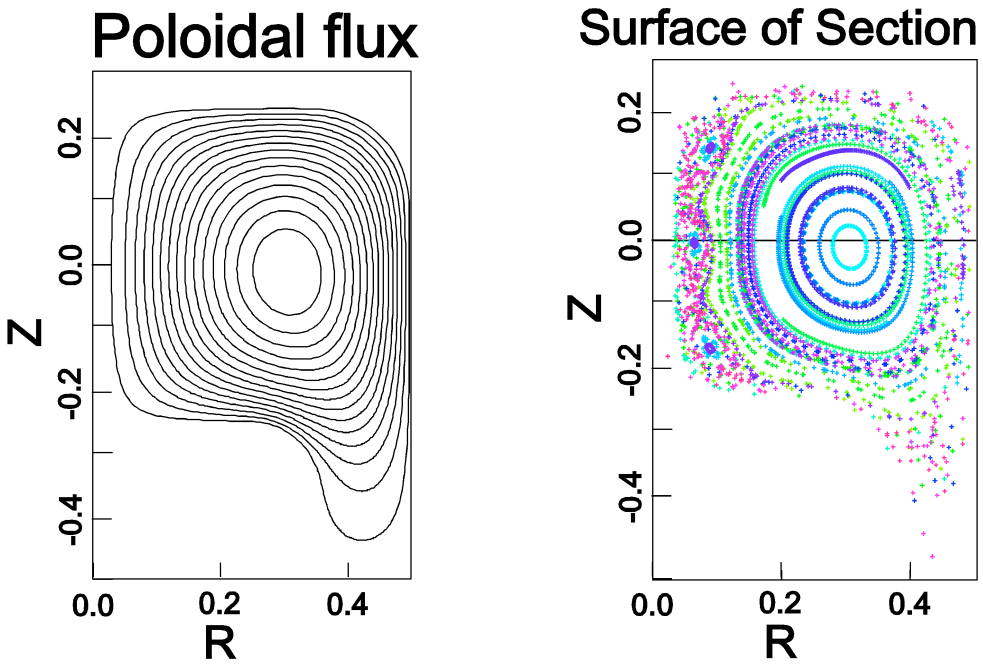

(a) (b)

Fig. 8. (a) Poloidal flux surfaces for the mean-field spheromak at 2 ms. (b) Poincaré plot for the full magnetic configuration at 2 ms showing the breaking of magnetic surfaces near the separatrix. {Reflux-deflux/RefluxBA-def_524666_polfl.tif, pss.tif}

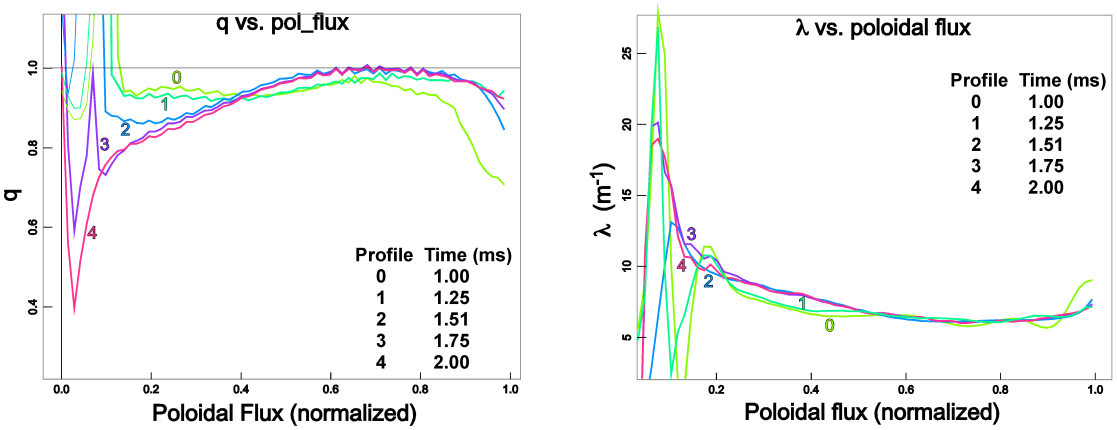

Fig. 9. Safety factor and l profiles at several times throughout the simulation. (a) and (b) During the deflux phase. {Reflux-deflux/q-profiles}

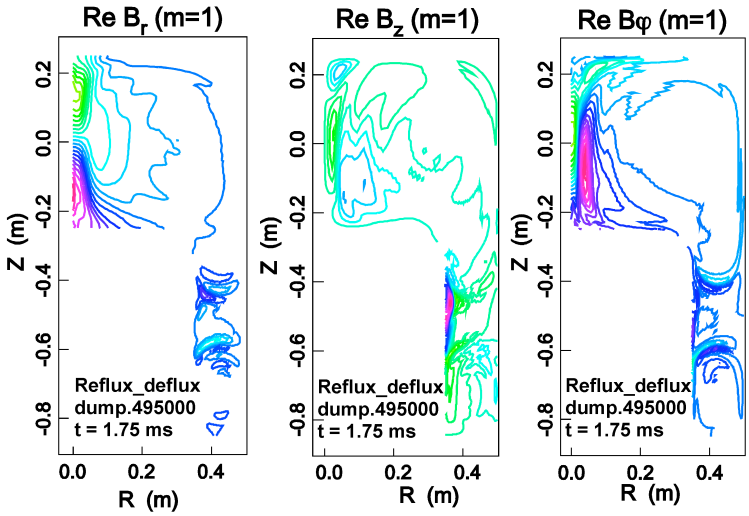

Fig. 10. Activity of the n=1 mode at 1.75 ms. {Reflux-deflux/q-profiles/Reflux_deflux_495000_B-m=1.tif}

B. REDUC-12 (IPM)

As in the NIMROD simulation, the gun flux and current are reduced at constant λ_s. between 1.0 and 2.0 ms. There is one complication: as seen in Fig. 8 there is a volume inside the separatrix in which the MHD activity is large enough to generate islands and stochastic field lines. To model this, we form an edge (boundary) layer in which the hyper-resistive coefficient is maintained as large as the value used in the buildup phase. The coefficient is reduced smoothly from the plasma edge (in Corsica) to a reduced value at a relative minor radius of 0.6. The reduction is smooth between 0.67 and 0.6. An example is shown in Fig. 11a. The value of Λ in the core plasma is reduced during the ramp-down time to a value $< 10^{-4}$ V-Wb as shown in Fig. 11b. The thermal conductivity is also ramped down in the core with a profile and time history similar to Λ. The resulting temperature spatial variation at 2 ms is shown in Fig. 12.

The flux evolution during ramp-down as calculated by the integrated model is compared with the NIMROD simulation in Fig. 13a, and the temperature is shown in Fig. 13b. The model for the flux overshoots a bit and the temperature is a bit low during most of the ramp-down, but the fit is qualitatively reasonable. It is clear that including the stochastic layer around the separatrix is a critical part of describing the flux and temperature evolution during this period, as they reduce the effective minor radius of the spheromak. They will also be needed in modeling the slow decay following the ramp down.

The safety factor in the IPM, Fig. 14, goes above unity at 1.5 ms. There is no mechanism in the model to keep $q < 1$, unlike the resistive MHD model in which a n=1, m=1, activity is expected. The IPM thus is consistent with the simulation; together they supports an interpretation in which a low-level, n=1, m=1 column instability, seen in Fig. 10, exists which keeps the safety factor below unity throughout the plasma, presumedly coupling strongly to the plasma near the magnetic axis as q approaches unity and "clamping" the q-profile < 1.

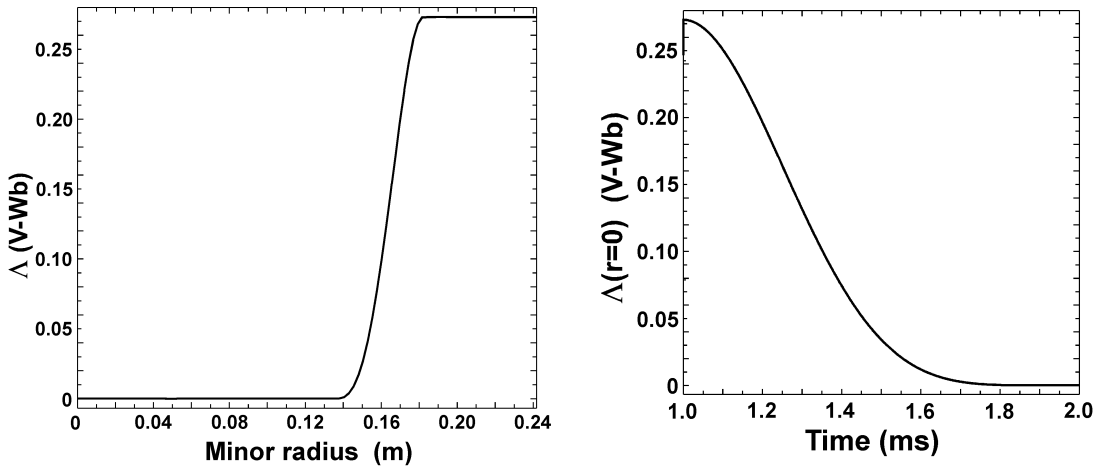

(a) (b)

Fig. 11. (a) Spatial variation of Λ; this example has a very small Λ in the plasma core. (b) Time history of Λ in the plasma core. The minor radius is defined as 0.5 time the difference in major radii at the horizontal midplane of the spheromak. {hilam_spitzI/hilam_spitzI_lam_prof.tif, hilam_spitzI_lam-norm_hst.tif}

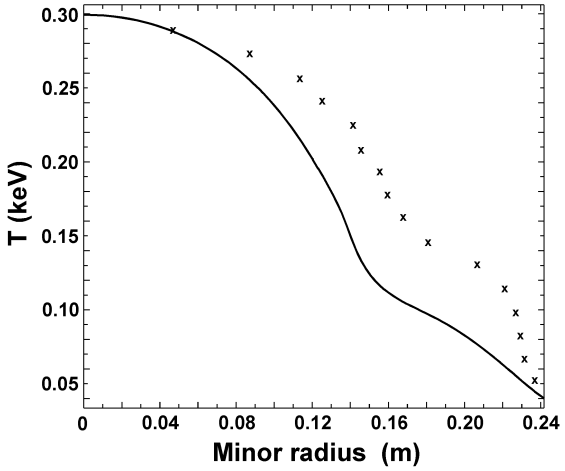

Fig. 12 The spatial variation of temperature at 2.0 ms. The x points are from the NIMROD simulations and the solid line from the integrated model. The integrated model was fit to 0.3 keV at r = 0. {hilam_spitzI/hilam_spitzI_T-rmin.tif}

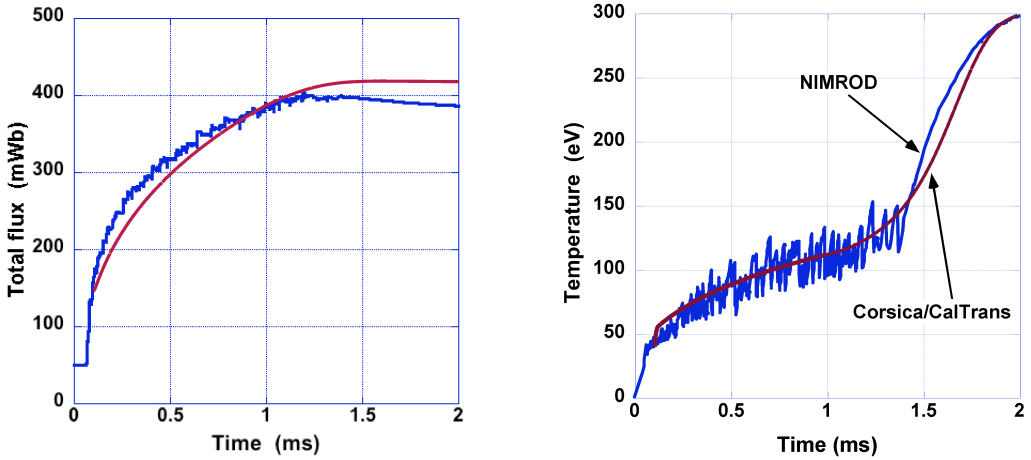

(a) (b)

Fig. 13. (a) The flux evolution and (b) temperature on the magnetic axis during buildup and ramp down. {hilam_spitzI/Reflux+defluxA.tif, hilam_spitzI/Reflux-Tmax.cvx}

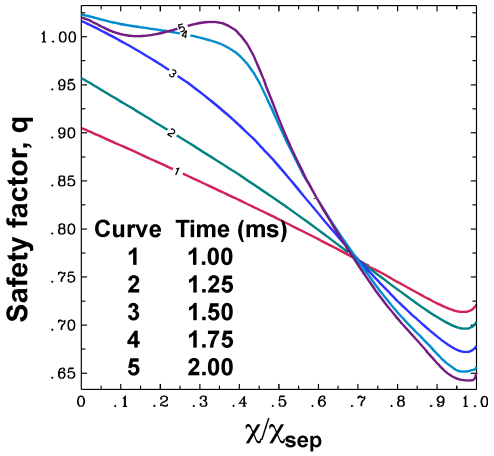

Fig. 14. Safety factor, q, between 1.0 and 2.0 ms. {Reflux-deflux/q-profiles/hilam_spitzQ_q-profiles.tif}

C. REDUC-21 (IPM)

Before running another simulation, the IPM was exercised to estimate optimum parameters. Two variations were considered: (1) Reduce λ_g before the reduction of gun (bias) flux and current at constant λ_g, and (2) Varying the final value of λ_g to ensure that q is large but <1. The results from the variation of λ_g are shown in Fig. 15. The q-profile in the core plasma as found using the integrated physics model are in an optimum range for minimizing internal, low-order rational surfaces. It was, therefore, chosen for the second resistive MHD simulation. Note that this is higher than the value, ≈ 9 m^{-1} which maximized the temperature in SSPX; however, the open fieldlines fill a much smaller volume (relative to that available in the flux conserver)

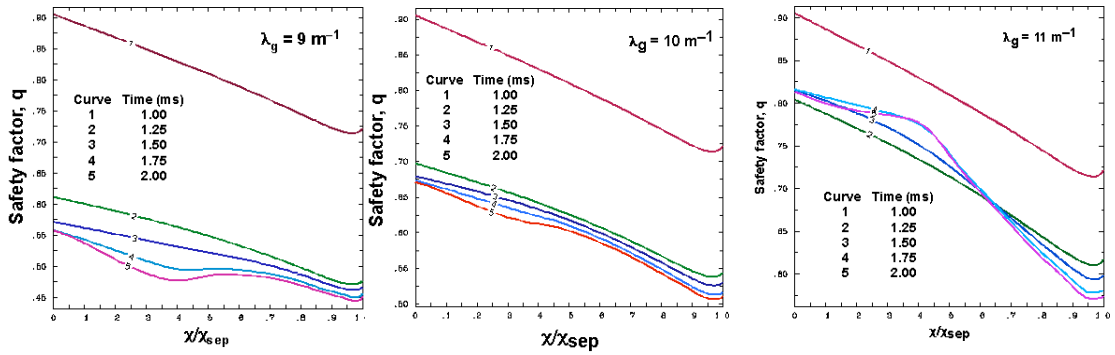

(a) (b) (c)

Fig. 15. λ -profiles for several times during the reduction in λ_g and the deflux phase for λ_g = 9, 10, and 11 m^{-1}. The drop between 1.00 and 1.25 ms results from the decrease in λ_g from its starting value during the interval $1.0 \le t \le 1.1$ ms. {Lam_q-t/lam_gC2_q-t.tif, lam_gA_q-t.tif, lam_gB2_q-t.tif.}

Controlled decay

Starting at 2 ms, the plasma was allowed to decay. As $\lambda_{gun} = 25\ m^{-1}$ at 2 ms was still greater than the flux conserver eigenvalue, $\lambda_0 = 10\ m^{-1}$, the gun current was reduced over the first 0.1 ms of this phase to yield λ_0. The resulting boundary condition helps maintain a nearly constant λ in the spheromak volume, reducing the drive for MHD instabilities. The thermal conductivity was decreased to 5 m^2/s, closer to the measured experimental values and to obtain more data on the behavior of the thermal confinement in the model. The simulation was carried out to t > 3 ms before ended for reasons discussed below. Fig. 16a shows the results, a slow decay as one would expect.

Figure 16b compares the temperature rise after 2 ms with that from a purely axisymmetric simulation starting at the same point. The temperature rise resulting when the mode n=1-5 are included is considerably less than in the axisymmetric approximation, where flux surfaces are "perfect" and there is no region of stochastic field lines. For the case including the higher-order modes, the Poincaré plot is similar that shown in Fig 8b, and the reduced temperature rise seen in Fig. 16b is consistent with the effective reduced minor radius for good flux surfaces.

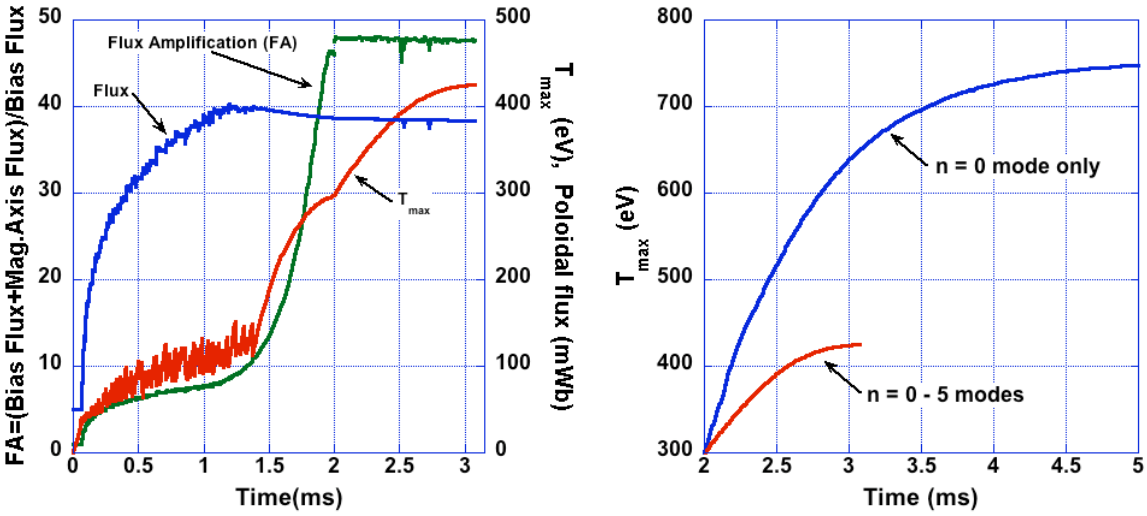

(a) (b)

Fig. 16. Extension of the simulation to include the slow decay that results when λ_{gun} is reduced to 10 m^{-1}. {Reflux-decay/RefluxBA2.tif, T - n=0 and n=0-5 modes.tif }

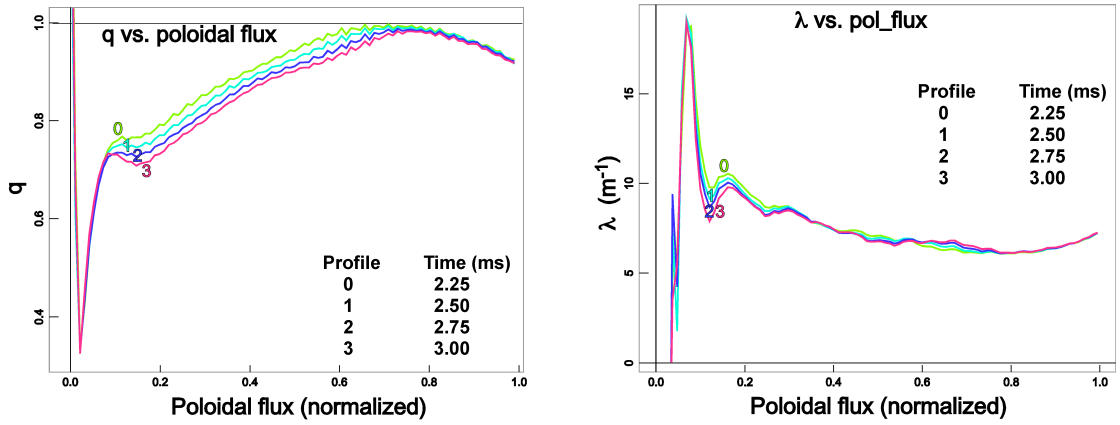

(c) (d)

Fig. 17. Safety factor and l profiles at several times throughout the simulation. (a) and (b) During the deflux phase. {Reflux-deflux/q-profiles} (c) and (d) During the controlled decay phase. {Reflux-decay/q-profiles}

Examination of the safety factor in the simulated plasma find that it is just below unity in the spheromak core, as seen in Fig. 17. Calculations using an integrated physics model (IPM) indicate that that reducing the flux and current at fixed λ_g result in the core plasma current being nearly frozen-in when the value of λ_g is later reduced, resulting in an increase of q above unity in the axisymmetric approximation. Although no reconnections are observed in the 3D simulations and flux surfaces are closed in the core, the observation that q sits just below unity suggests that low-level MHD activity may be playing a role in maintaining $q < 1$. We will explore this in a second NIMROD simulation discussed later in this document.

The simulation has difficulties both with the long computational times required and the spatial resolution required to resolve the current column along the geometric axis. The grid size used in the calculation has a typical radial dimension of about 2 cm along the geometric axis; in the gun the dimension is about 0.6 cm. The effective resolution is improved by the use of finite elements [21]. "Standard" simulations in the SSPX geometry use bicubic elements [22] which are found to provide a reasonable trade-off between computational time and accuracy. The accuracy decreases at the highest mode number, n=5, but this has been found to have little effect on the important physics. However, in the present case, the excited modes near the separatrix include a large amplitude n=5. Increasing the finite element to biquartic caused only small differences in the amplitude of this mode or the temperature in the core of the plasma, but slowed the calculation further. Accordingly, the simulation calculation was terminated at 3.23 ms. The results were used to form a physics model, discussed below, to allow modeling for longer times, to provide a means of interpreting the NIMROD results, and to allow for exploring the effect of parameter variations on the refluxing scenario.

Integrated modeling results

Decay phase

The final phase in the spheromak evolution is the slow decay with no current drive until the next refluxing pulse is applied. The constant part of the thermal conductivity was reduced to 10 m^2/s as in the Nimrod simulation. Results to t ≈ 3 ms are shown in Fig. 18 where they are compared with the simulation. The final temperature is a bit low as the contribution to the thermal

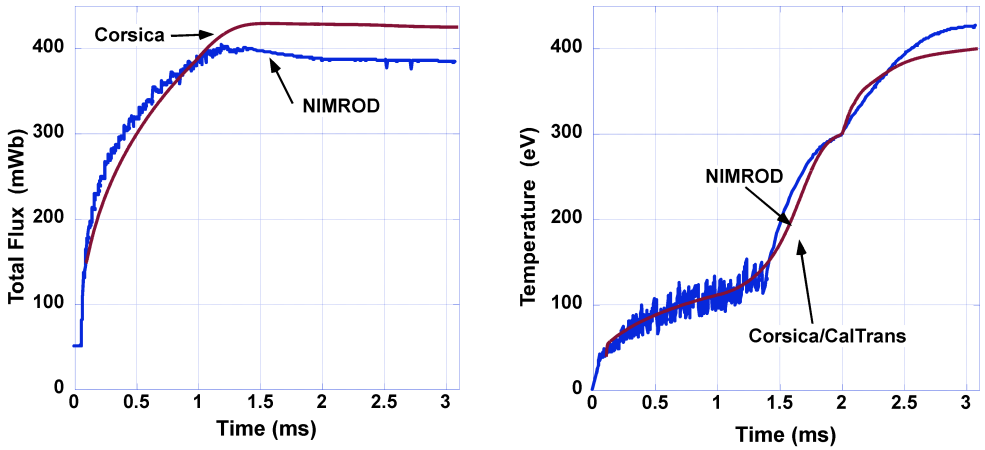

(a) (b)

Fig. 18. (a) Flux evolution and (b) temperature evolution for t ≤ 3 ms. {Reflux-decay/Total flux.tif, Reflux-decay/decay_T-t.tif}

conductivity was not reduced quite to zero in this particular calculation. This could have been corrected, however this modeling revealed the continuation of a more serious difficulty: The safety factor, q, was greater than unity during the deflux and decay phase; see Figs. 14 and 18.

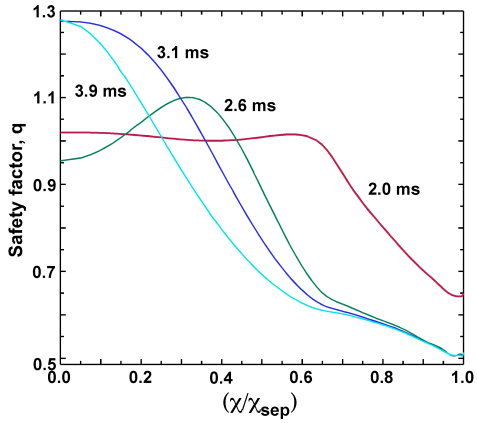

Fig. 19. Safety-factor profile during the decay phase. Each profile is labeled with the time. Note that for the IPM as used here, the value of q was not required to be < 0, e.g. by turning on localized hyper-resistivity as was done for modeling sawteeth in the tokamak in Ref. 23. {Reflux-decay/decayG1_qTor.tif}

Integrated modeling: Alternative ramp-down scenario

In the results that resulted in the safety-factor profiles shown in Fig. 15, the rate of change of the plasma current in the (relatively) hot spheromak core is much slower than that of the edge, resulting in q > 0 in the plasma. These results can be compared with those from Nimrod in Fig. 17. This raises the issue of timing in the transition to a decaying plasma. In the Nimrod run for $\lambda_g = 10$ m^{-1}, the first step was to reduce the gun current and bias flux together at constant l, followed by reducing λ_g. In order to examine whether this order matters, the IPM was run for the reversed ordering during the transition, with the result shown in Figs. 15 and 21.

There is a clear difference within the IPM. It also suggests that the optimum value for λ_g is about 11 m^{-1} as that gives a q-profile between 0.75 and 1. However, as we will see, the Nimrod runs behave somewhat differently, suggesting that the order of the two transition phases is not critical and that the best value for λ_g is about 10 m^{-1}. The reasons are not completely clear, but the physics preventing $q = 1$ may be part of the cause.

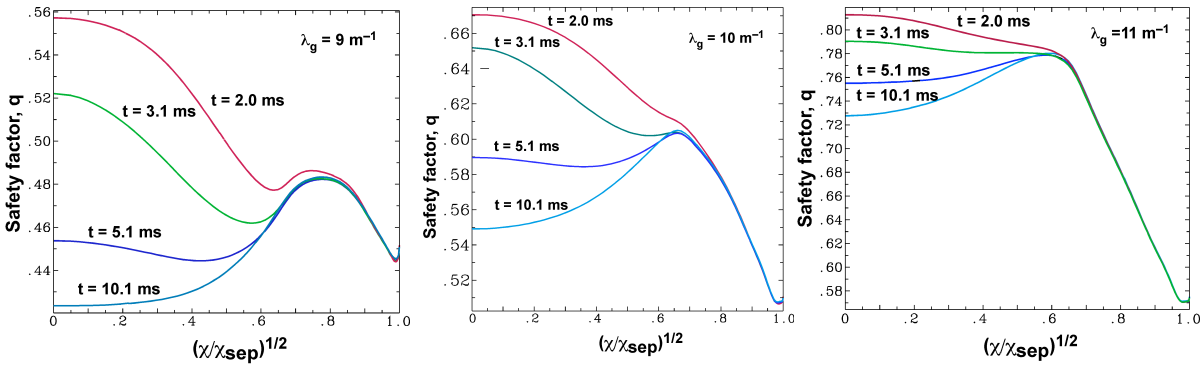

Fig. 22. Safety-factor profiles during the transition after the reduction in λ_g when it is done before the reduction of gun current and flux. {Lam_q-t/lam_gC2_decay_q-t.tif, lam_A2_decay_q-t.tif, and lam_gB2_decay_q-t.tif.}

Comments on profile control

It is clear that the spheromak is quite sensitive to the q-profile, both in the plasma interior and in the region around the separatrix. The value of λ_s has a significant impact on the profile, but it does not do the same job that localized current drive would do. Although this study does not undertake a detailed study of the options, some are briefly summarized here.

Neutral beam current drive. Studies [9, 10] primarily focussed on using neutral beams as a steady-state current drive, concluding that it may be possible to access a q-profile which yields a stable state. Ref. 9 did some exploration of the effect of varying the beam aiming, and showed that the q-profile was effected, but did not consider the effects of transport. Fowler concluded that power requirements for a reactor may be satisfactory [10, 24] and that stable profiles may be accessible Generally, however, the large orbits [9] make it useful for affecting the profile across most of the radius but difficult to use for localized control or for control of tearing modes.

Electron Bernstein current drive. Highly localized current drive in the tokamak uses ECCD, that is, waves that have an electron cyclotron resonance (or second harmonic) at the location of interest. However, in overdense plasmas including the spheromak (and STs) where the plasma frequency is greater than the cyclotron frequency there is no access for ECRH. However, electron Bernstein waves have been demonstrated to drive localized current [25, 26, 27, 28] and the theory of the drive is fairly well understood [29, 30, 31]. The experimental application of these waves for localized current drive for spheromaks has not been attempted, but they are a natural tool for local control of the MHD modes.

This work performed under the auspices of the U.S. Department of Energy by Lawrence Livermore National Laboratory under Contract DE-AC52-07NA27344.

Appendix: Integrated physics model for the refluxing scenario

The integrated physics model is based on the Corsica code, which solves the Grad-Shafranov equation coupled to heating, current drive, and transport models ("Caltrans" [16, 17]). The MHD description is axisymmetric and thus describes a mean-field spheromak together with models for heating and transport, current drive, all of which may include non-axisymmetric effects. These models, which are generally based on published physics analysis, typically have one (or a small number) of parameters which are not known from first principles. In the present modeling the parameters are chosen by fitting the time history of the plasma evolution to that in the Nimrod simulation. The success of the model is judged by the quality of that fit and the reasonableness of the parameter values, with the latter judged both from the simulation and the SSPX experiment.

Current drive

The current drive used for helicity injection into the spheromak is approximated by an hyper-resistive model as given by Boozer. This model has previously been used to describe the plasma buildup in SSPX, with the hyper-resistive diffusion coefficient the only free parameter [18]. In that calculation the electron temperature was assumed constant, with a value from experimental discharges. For our present work we include heating due to the effective hyper-resistive electric field.

Boozer's result can be written as

$$\eta \mathbf{j} = \mathbf{E} + \mathbf{v} \times \mathbf{B} + \frac{\mathbf{B}}{B^2} \nabla \cdot \left(\Lambda \nabla \lambda \right) \qquad (1)$$

(Our notation differs from Boozer's. Here, $\lambda = \mu_0 \mathbf{j} \cdot \mathbf{B} / B^2$.) The implementation of this model in Corsica is discussed in Ref. [32]. The value of Λ is one of our fitting parameters and in general is a flux function.

As this approximation essentially assumes fine-grained turbulence, it cannot reproduce the spiking voltage and "sawtooth-like" temperature history, and has to be interpreted as a time-averaged current and flux drive. As found previously [32] and as seen below, however, even the simplest model with a constant Λ does a surprisingly good job of reproducing the time-dependent buildup of current averaged over the reconnection events. During the "controlled-decay" mode, it will be assumed to hold in an edge plasma which extends inside the mean-field separatrix, as seen in the Nimrod simulations. Inside the edge region, the value of Λ will be reduced to a small enough value that it has negligible effect on the spheromak.

Plasma heating

The temperature moment equation in the single-fluid, resistive MHD approximation is used in NIMROD in the form [22]:

$$\frac{nk_B}{\gamma-1}\left(\frac{\partial T}{\partial t}+\mathbf{V}\cdot\nabla T\right)=-\frac{p}{2}\nabla\cdot\mathbf{V}+\nabla\cdot nk_B\left[\chi_{\parallel}\hat{\mathbf{b}}\hat{\mathbf{b}}+\chi_{\perp}\left(\mathbf{I}-\hat{\mathbf{b}}\hat{\mathbf{b}}\right)\right]\cdot\nabla T+\frac{\eta j^2}{2} \tag{2}$$

The first term on the rhs corresponds to compressional heating and the second to thermal losses along and across the magnetic field.

Within resistive MHD, Ohms law is

$$\eta\mathbf{j}=\mathbf{E}+\mathbf{v}\times\mathbf{B} \tag{3}$$

In the hyper-resistive approximation, we write this as

$$\eta\mathbf{j}=\mathbf{E}+\mathbf{v}\times\mathbf{B}+\left\langle\tilde{\mathbf{v}}\times\tilde{\mathbf{B}}\right\rangle \tag{4}$$

where the average is over the (assumed) fine-grained turbulence, represented by the tilde, and terms without the tilde are averaged quantities. We take the average as equivalent to the azimuthal average of the fluctuating quantities, denoting the average of the turbulence by $\left\langle\tilde{\mathbf{v}}\times\tilde{\mathbf{B}}\right\rangle_{\varphi}$. Equating this average to Boozer's result yields his hyper-resistive model with $\left\langle\tilde{\mathbf{v}}\times\tilde{\mathbf{B}}\right\rangle_{\varphi}=\mathbf{B}/B^2\nabla\cdot\left(\Lambda\nabla\lambda\right)$.

The ohmic heating term in Eq. (2) can be written

$$\begin{aligned}\left\langle\eta j^2\right\rangle_{\varphi}&=\left\langle\mathbf{j}\cdot\mathbf{E}\right\rangle_{\varphi}+\left\langle\mathbf{j}\cdot\mathbf{v}\times\mathbf{B}\right\rangle_{\varphi}\\&=\left[\mathbf{j}\cdot\left(\mathbf{E}+\mathbf{v}\times\mathbf{B}\right)+\mathbf{j}\cdot\left\langle\tilde{\mathbf{v}}\times\tilde{\mathbf{B}}\right\rangle_{\varphi}\right]+\left(\left\langle\tilde{\mathbf{j}}\cdot\tilde{\mathbf{E}}\right\rangle_{\varphi}-\mathbf{v}\cdot\left\langle\tilde{\mathbf{j}}\times\tilde{\mathbf{B}}\right\rangle_{\varphi}+\mathbf{B}\cdot\left\langle\tilde{\mathbf{j}}\times\tilde{\mathbf{v}}\right\rangle_{\varphi}+\left\langle\tilde{\mathbf{j}}\cdot\tilde{\mathbf{v}}\times\tilde{\mathbf{B}}\right\rangle_{\varphi}\right)\end{aligned} \tag{5}$$

The terms inside the square brackets are included in the hyper-resistive ohm's law, but those inside the curved brackets are not. The latter include the strong ion heating often observed in helicity-driven discharges including SSPX [33, 34] as well as other physics missing in our model. They are included in the NIMROD simulation to the extent they can be described in a single-fluid MHD approximation, but are not included in our present integrated model approximation. Thus, we approximate the heating as

$$\begin{aligned}\left\langle\eta j^2\right\rangle_{\varphi}&=\mathbf{j}\cdot\left(\mathbf{E}+\mathbf{v}\times\mathbf{B}\right)+\mathbf{j}\cdot\left\langle\tilde{\mathbf{v}}\times\tilde{\mathbf{B}}\right\rangle_{\varphi}\\&=\mathbf{j}\cdot\left(\mathbf{E}+\mathbf{v}\times\mathbf{B}\right)+\frac{\lambda}{\mu_0}\nabla\cdot\left(\Lambda\nabla\lambda\right)\end{aligned} \tag{6}$$

The last term can be interpreted as due to ohmic heating in the local frame moving with the turbulence and is additive to the heating (or cooling) resulting from the azimuthally-averaged loop voltage. As we will see below, the second derivative of λ is > 0 throughout most of the spheromak during buildup with Λ = constant, so this heating term corresponds to power flow inward from the plasma edge resulting in a net volume-integrated $\left\langle\eta j^2\right\rangle_{\varphi}$. This interpretation differs from that of Boozer.

Thermal conductivity

Transport of magnetic helicity across any closed surface requires that field lines cross that surface; resulting in magnetic flux surfaces which are closed only in the mean-field approximation [35, 36, 37]. In the same spirit that we assume that the current drive is a time-average over any bursting or sawtooth-like

behavior, we use a time-averaged model for the thermal conductivity. In particular, our model uses a Rechester-Rosenbluth thermal conductivity approximation:

$$\chi_{\perp} = 0.5 \mathrm{v}_e \left|\delta B/B\right|^2 = 6.6 \times 10^6 \sqrt{T} \left|\delta B/B\right|^2 \quad (7)$$

with temperature in keV. A single parameter, $\left|\delta B/B\right|$, will be found to give a reasonably good result for the thermal evolution in stochastic magnetic fields in the mean-field spheromak.

1. M. N. Rosenbluth and M. N. Bussac, Nucl. Fusion **19**, 489 (1987).
2. T. R. Jarboe, et al., Phys. Fluids B **2**, 1342 (1990).
3. B. Hudson, et al., Phys. Plasmas **15**, 056112 (2008).
4. T. R. Jarboe, Plasma Phys. Control. Fusion **36**, 945 (1994).
5. H. S. McLean, et al. Phys. Rev. Letters **88**, 125004 (2002).
6. H. S. McLean, et al., Plasma Phys. **13**, 056105 (2006).
7. E. B. Hooper, et al., Phys. Plasma **12**, 092503 (2005).
8. B. I. Cohen, et al., Phys. Plasmas **16**, 042501 (2009).
9. A. F. Lifschitz, R. Farengo, and N. R. Arista, Plasma Phys. Control. Fusion **44**, 1979 (2002).
10. T. K. Fowler, et al. J. Fusion Energy **28**, 118 (2009).
11. E. B. Hooper, et al., Nucl. Fusion **47**, 1064 (2007).
12. R. D. Wood, et al., Nucl. Fusion **49**, 025001 (2009).
13. R. L. Hagenson and R. A. Krakowski, Fusion Tech. **8**, 1606 (1985).
14. C. R. Sovinec, et al., Phys. Rev. Letter **94**, 035003 (2004).
15. B. I. Stallard, et al., Phys. Plasmas **10**, 2912 (2003).
16. E. B. Hooper, L. D. Pearlstein, and R. H. Bulmer, Nucl. Fusion **39**, 863 (1999).
17. J. A. Crotinger, et al., "Corsica: A Comprehensive Simulation of Toroidal Magnetic-Fusion Devices," LLNL Report UCRL-ID-126284 (June 12, 1997).
18. A. H. Boozer, J. Plasma Phys. **35**, 133 (1986).
19. A. B. Rechester and M. N. Rosenbluth, Phys. Rev. Letters **40**, 38 (1978).
20. E. B. Hooper, et al., Phys. Plasmas **15**, 032502 (2008).
21. C. R. Sovinec, et al., J. Comp. Phys. **195**, 355 (2004).
22. B. I. Cohen, et al., Phys. Plasmas **12**, 056106 (2005).
23. D. J. Ward and S. C. Jardin, Nucl. Fusion **29**, 905 (1989).
24. T.K. Fowler, A development path for the stabilized spheromak reactor, Lawrence Livermore National Laboratory report UCRLTR-232757 (2007)
25. V. Shevchenko, et al., Phys. Rev. Letters **89**, 265005 (2002).
26. H. P. Laqua, H. Maassberg, N. B. Marushchenko, F. Volpe, A. Weller, and W7-AS Team, Phys. Rev. Letters **90**, 075003 (2003).
27. A. Meuck, A. Camenen, S. Coda, et al., Fusion Science and Technology **52**, 221 (2007).
28. A. Pochelon, A. Mueck, L. Curchod, et al., Nucl. Fusion **47**, 1552 (2007).
29. H. P. Laqua, Plasma Phys. Control. Fusion **49**, R1 (2007).
30. J. M. García, F. Castejón, A. Cappa, N. B. Marushchenko, and M. Tereshchenko, Plasma Phys. Control. Fusion **52**, 1 (2010).
31. G. Taylor, P. C. Efthimion, C. E. Kessel, et al., Phys. Plasmas **11**, 4733 (2004).

32. E. B. Hooper and L. D. Pearlstein, Plasma Phys. Reports 28, 765 (2002).
26. D. W. Auerbach, D. N. Hill, and H. S. McLean, "Ion Temperature Measurements in SSPX," LLNL Report UCRL-ID-145235 (August 24, 2001).
27. E. D. Mezonlin, et al., Rev. Sci. Instrum. **78**, 053504 (2007).
28. A. H. Boozer, Phys. Fluids B **5**, 2271 (1993).
29. R. W. Moses, R. A. Gerwin, and K. F. Schoenberg, Phys. Plasmas **8**, 4839 (2001).
30. R. R. Mett and J. B. Taylor, Phys. Fluids B **4**, 73 (1991).